Supplementary Information

Operando Characterization of Lithium Battery Internal Temperatures via Upconverting Nanoparticle Thermometry

Fei Hu [a,†], *Ziyang Ye* [b,†], *Andrea D. Pickel* [b, c,*] *and Wyatt E. Tenhaeff* [a,*]

[a] Department of Chemical Engineering, University of Rochester, Rochester, New York 14627, USA.

[b] Materials Science Program, University of Rochester, Rochester, New York 14627, USA.

[c] Department of Mechanical Engineering, University of Rochester, Rochester, New York 14627, USA.

[†] Fei Hu and Ziyang Ye contributed equally.

AUTHOR INFORMATION

Corresponding Author

*Andrea D. Pickel (apickel@ur.rochester.edu)

*Wyatt E. Tenhaeff (wyatt.tenhaeff@rochester.edu)

a

Spots	A	ΔE (meV)
1	8.0168	90.1
2	7.9092	89.7
3	8.0403	90.1
4	8.1223	90.4
5	8.1334	90.5

b

Spots	A	ΔE (meV)
1	8.0534	90.6
2	7.9602	90.3
3	7.9261	90.2
4	7.9335	90.2
5	7.9877	90.5

c

Spots	A	ΔE (meV)
1	9.6711	94.8
2	9.3597	93.9
3	9.7847	95.2
4	9.4610	94.2
5	9.4748	94.2

Table S1. Fitted A and ΔE values corresponding to ratiometric thermometry calibrations performed for five different spots on different substrates: **a** MnO_2 (cathode), **b** glass fiber (separator), and **c** Li metal (anode)

Component	**Materials**	**Thickness (µm)**	**Thermal conductivity (W/m·K)**
Coin Cell Case	Stainless Steel[1]	270 (bottom), 1350 (top)	15
Cathode	MnO_2[2]	1350	0.65
Separator Saturated with Electrolyte	Glass Fiber $LiPF_6$/EC/DMC/EMC	250	0.51
Anode	Li[3]	200	72

Table S2. Thermal conductivity of materials and thickness for each component in coin cell batteries tested in main text Figure 4. The thermal conductivity of the separator saturated with electrolyte is calculated using the parallel model of thermal resistance with an input porosity of 90% (as provided by Sigma Aldrich). The thermal conductivity values used are 1 W/m·K and 0.45 W/m·K for the glass fiber[4] and the $LiPF_6$/EC/DMC/EMC electrolyte[5], respectively.

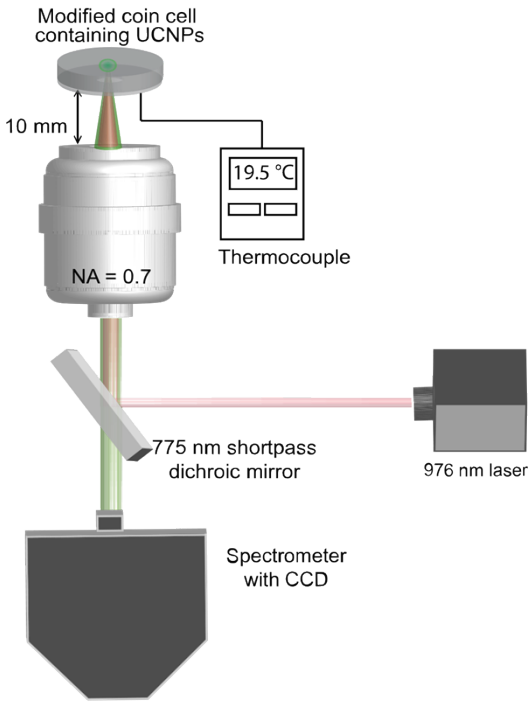

Figure S1. Illustration of custom-built microscopy and spectroscopy system for monitoring the internal and external temperature of the coin cells.

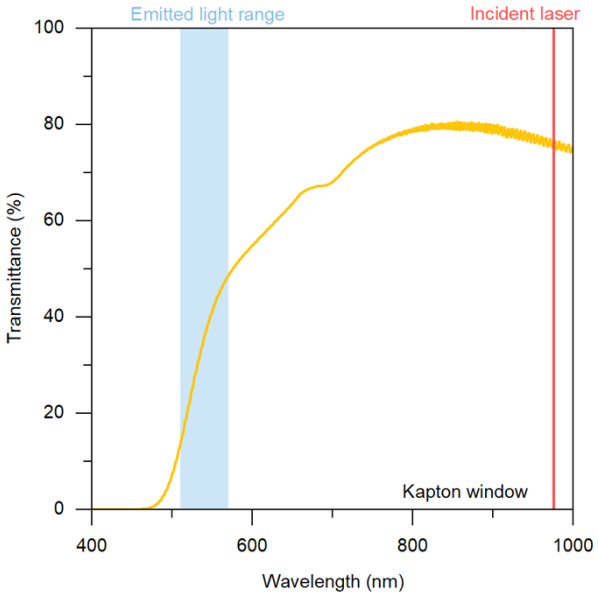

Figure S2. Transmittance spectrum of Kapton® film for wavelengths from 400 to 1000 nm, which includes the emitted light range (blue area) used for temperature measurement and incident laser light (976 nm).

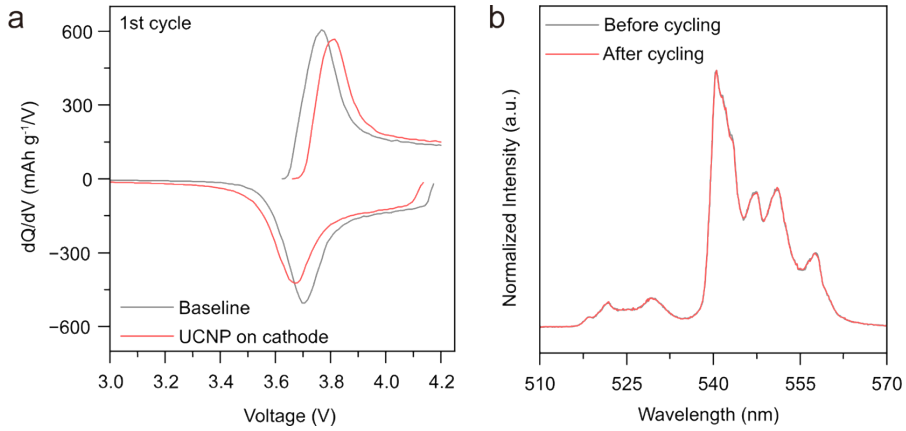

Figure S3. (a) Differential capacity (dQ/dV) analysis of NMC532-Li coin cells with and without UCNP on cathode at 1st cycle. (b) Luminescence spectra of NMC532-Li coin cells with UCNP on cathode before and after 50 cycles.

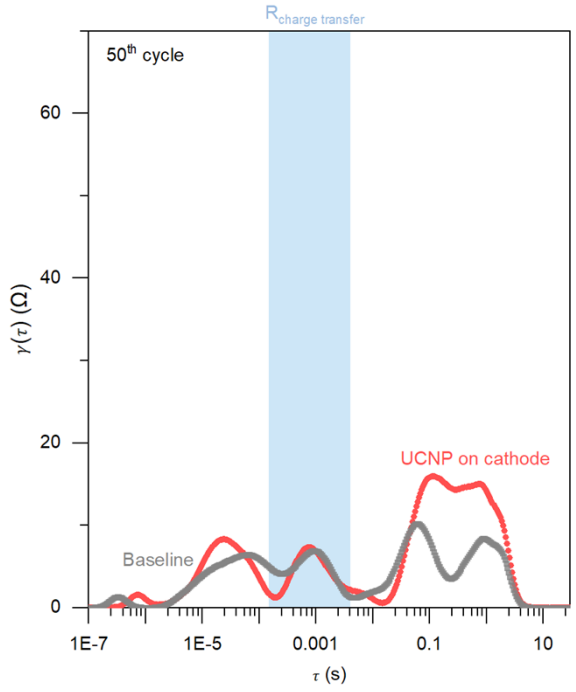

Figure S4. Distribution relaxation time (DRT) spectra of NMC532||Li coin cells with and without UCNP dispersed on the cathode, after 50 cycles.

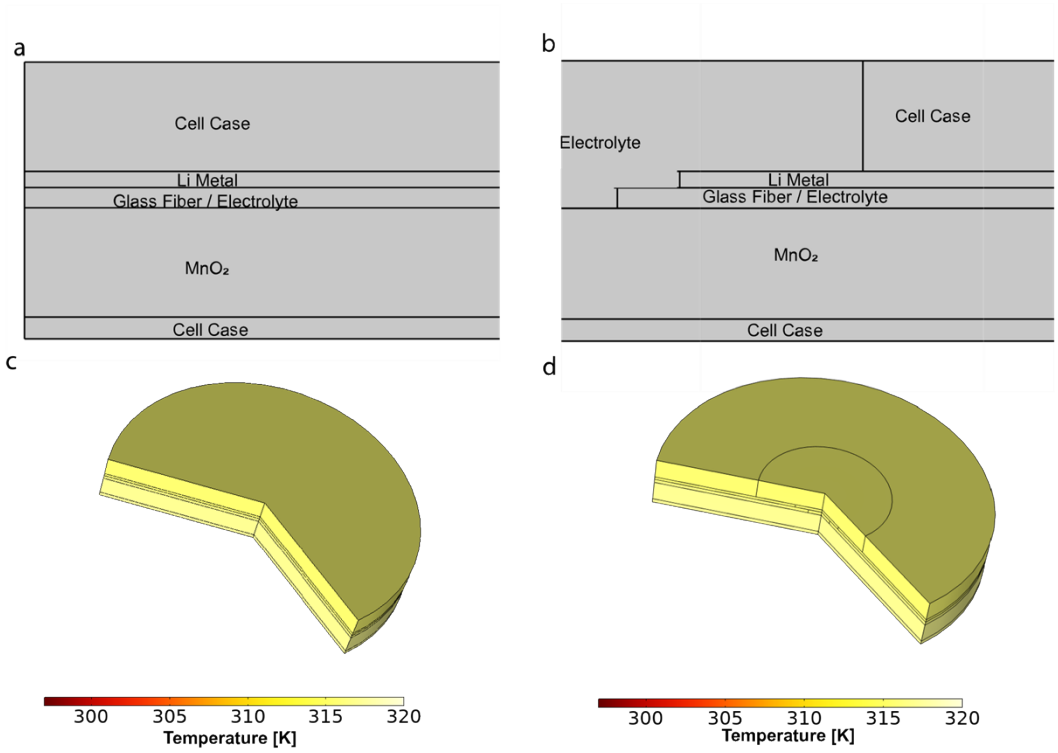

Figure S5. COMSOL heat transfer simulations for operating coin cell battery with and without optical path modification. (a) half of the unmodified coin cell structure and (b) half of the coin cell structure with optical path modification. The thermal conductivity and thickness of each layer are listed in **Table S2**. (c) and (d): 3D temperature distribution of the modified and unmodified coin cell.

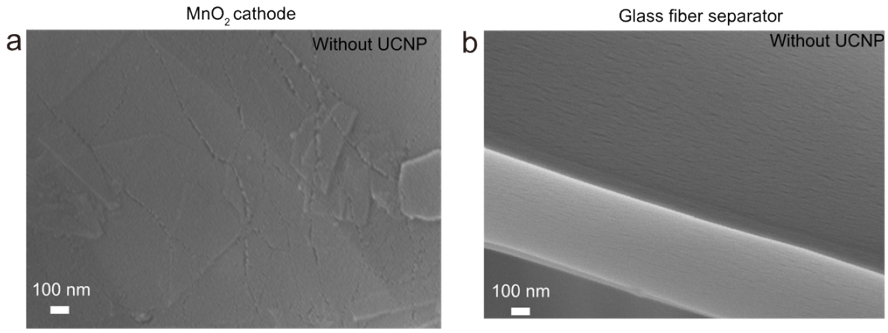

Figure S6. SEM images of a pristine (a) MnO_2 cathode and (b) glass fiber separator.

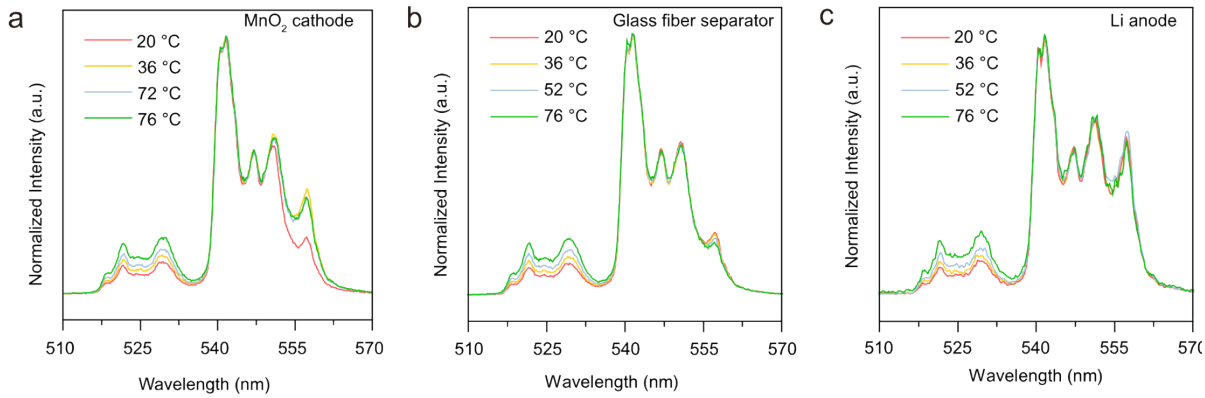

Figure S7. Luminescence spectra for temperature calibrations on (a) MnO_2 cathode, (b) glass fiber separator, and (c) Li anode for a temperature range of 20 °C to 76 °C.

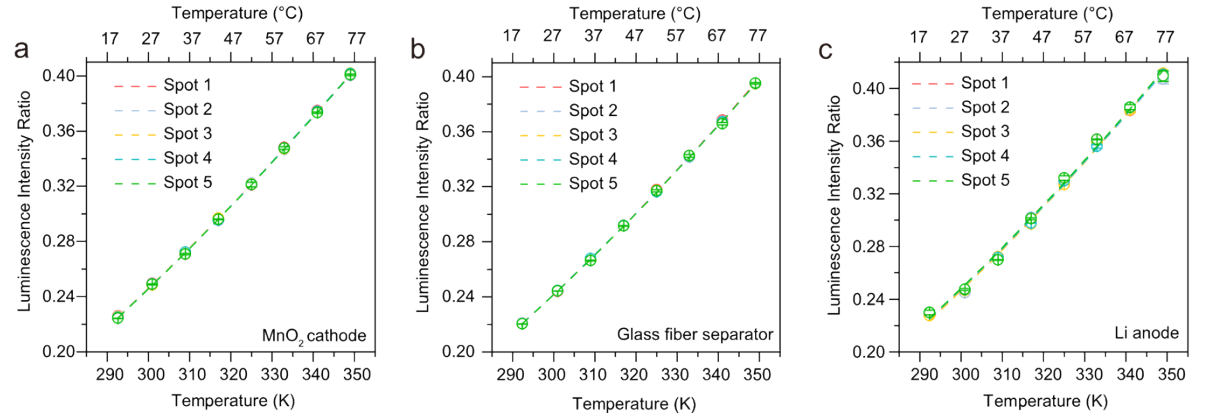

Figure S8. Luminescence intensity ratio calibrations on (a) MnO_2 cathode, (b) glass fiber separator and (c) Li anode for a temperature range of 20 °C to 76 °C.

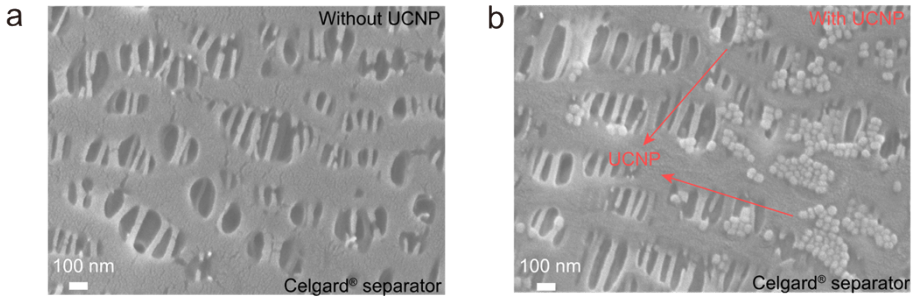

Figure S9. SEM images of Celgard® separator (a) before and (b) after UCNP deposition.

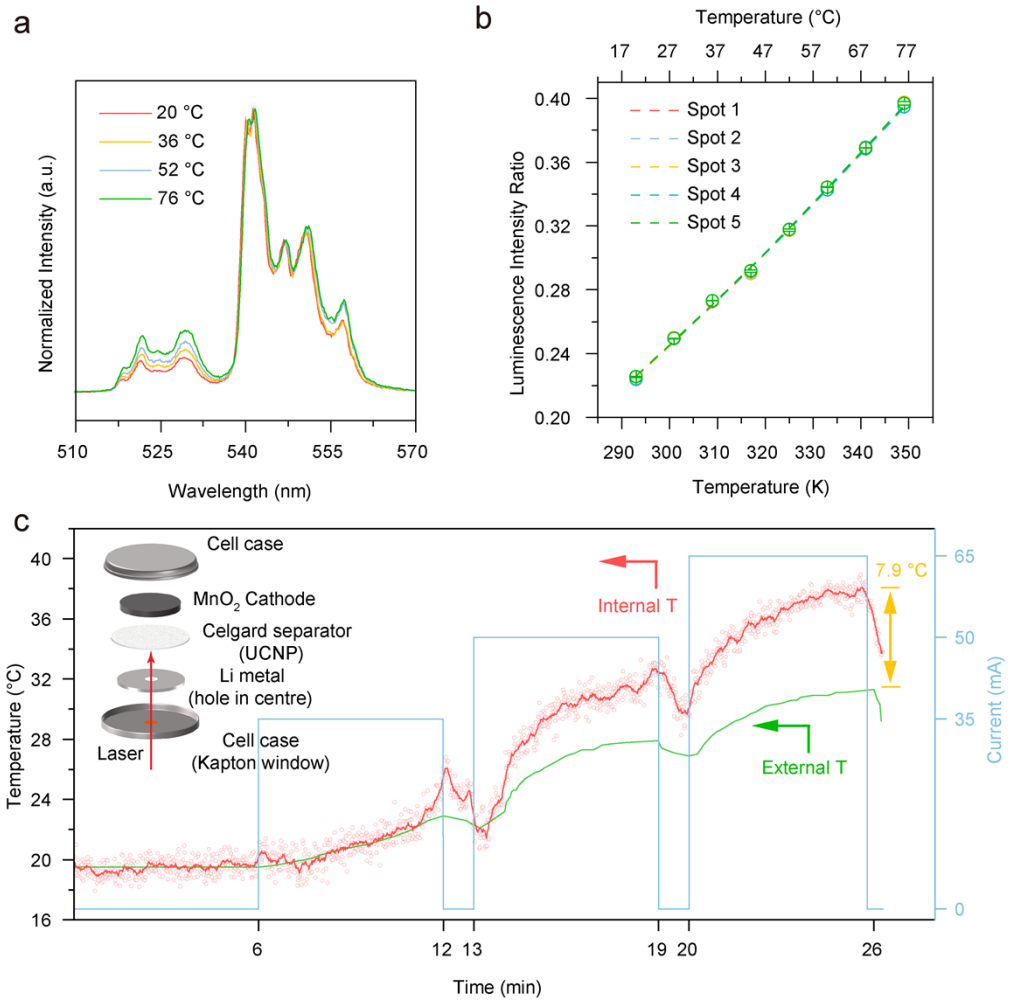

Figure S10. In-situ temperature evolution of MnO_2-Li coin cells as a function of time and current. UCNPs were put on the Celgard separator. (a) Luminescence spectrum of calibration sample at various temperatures. (b) Calibration curve of Celgard® 2325 separator with UCNPs at 5 different spots under various equilibrium temperatures. (c) In-situ temperature evolution at various external currents as a function of discharge/rest time.

Temperature resolution (°C)	Spatial resolution	Data acquisition time (s)	Accuracy (°C)	Temperature range (°C)
0.35	610 nm (ideal), sub-micrometer (estimated)	1.0	0.5	20 – 327*

Table S3. Comparative table for upconverting nanoparticle thermometry. The temperature resolution is defined as the smallest detectable temperature change with 1-second integration time, calculated by the standard deviation of the initial 6-minute temperature readout in Figure 4a of the main text. The ideal spatial resolution is calculated as $D = \lambda/(2 \times NA)$, where D is the spot size, λ is the excitation wavelength (976 nm), and NA is the numerical aperture of the objective (0.8). Temperature accuracy is calculated by taking the standard deviation of converted temperatures using five calibration curves and one input measured ratio. *For the temperature range: we conduct the calibration over a range from room temperature to 76 °C since this range is large enough for characterizing the temperature rise during the discharging process of the coin cells, but literature shows that thermometry using uncoated UCNPs is also feasible at higher temperatures up to approximately 327 °C.[6]

References

1. R. Graves, T. Kollie, D. McElroy and K. Gilchrist, *Int. J. Thermophys.*, 1991, **12**, 409-415.
2. A. Kumar, K. Kumari, C. Tomy and A. D. Thakur, 2020.
3. R. B. Ross, *Metallic materials specification handbook*, Springer Science & Business Media, 2013.
4. W.-Q. Lin, Y.-X. Zhang and H. Wang, *Science and Engineering of Composite Materials*, 2019, **26**, 412-422.
5. G. Guo, B. Long, B. Cheng, S. Zhou, P. Xu and B. Cao, *J. Power Sources*, 2010, **195**, 2393-2398.
6. R. G. Geitenbeek, P. T. Prins, W. Albrecht, A. van Blaaderen, B. M. Weckhuysen and A. Meijerink, *The Journal of Physical Chemistry C*, 2017, **121**, 3503-3510.